



# Kent Academic Repository

Xavier, Igor R.R., Giraldi, Gilson A., Gibson, Stuart James, Gattas, Gilka J.F., Rueckert, Daniel and Thomaz, Carlos E. (2019) *Age-related craniofacial differences based on spatio-temporal face image atlases*. IET Image Processing, 13 (9). pp. 1561-1568. ISSN 1751-9659.

## Downloaded from

<https://kar.kent.ac.uk/78978/> The University of Kent's Academic Repository KAR

## The version of record is available from

<https://doi.org/10.1049/iet-ipr.2018.6271>

## This document version

Author's Accepted Manuscript

## DOI for this version

## Licence for this version

UNSPECIFIED

## Additional information

## Versions of research works

### Versions of Record

If this version is the version of record, it is the same as the published version available on the publisher's web site. Cite as the published version.

### Author Accepted Manuscripts

If this document is identified as the Author Accepted Manuscript it is the version after peer review but before type setting, copy editing or publisher branding. Cite as Surname, Initial. (Year) 'Title of article'. To be published in *Title of Journal*, Volume and issue numbers [peer-reviewed accepted version]. Available at: DOI or URL (Accessed: date).

## Enquiries

If you have questions about this document contact [ResearchSupport@kent.ac.uk](mailto:ResearchSupport@kent.ac.uk). Please include the URL of the record in KAR. If you believe that your, or a third party's rights have been compromised through this document please see our [Take Down policy](https://www.kent.ac.uk/guides/kar-the-kent-academic-repository#policies) (available from <https://www.kent.ac.uk/guides/kar-the-kent-academic-repository#policies>).

# Age-related craniofacial differences based on spatio-temporal face image atlases

ISSN 1751-9659  
 Received on 2nd October 2018  
 Accepted on 29th April 2019  
 doi: 10.1049/iet-ipr.2018.6271  
 www.ietdl.org

Igor R.R. Xavier<sup>1</sup> ✉, Gilson A. Giraldi<sup>2</sup>, Stuart James Gibson<sup>3</sup>, Gilka J.F. Gattas<sup>4</sup>, Daniel Rueckert<sup>5</sup>, Carlos E. Thomaz<sup>1</sup>

<sup>1</sup>Department of Electrical Engineering, University Centre FEI, Sao Paulo, Brazil

<sup>2</sup>Department of Computer Science, National Laboratory for Scientific Computing, Rio de Janeiro, Brazil

<sup>3</sup>School of Physical Sciences, University of Kent, UK

<sup>4</sup>Department of Forensic Medicine, University of Sao Paulo, Sao Paulo, Brazil

<sup>5</sup>Department of Computing, Imperial College London, UK

✉ E-mail: cet@fei.edu.br

**Abstract:** A number of studies have been developed recently in order to explore associations between craniofacial differences and genetics. Most of these works have been based on spatial face image models, adjusted for the counter effects of age. This approach provides a limited understanding of normal and abnormal craniofacial development owing to the lack of age progression information. Here, the authors propose and implement an imaging framework that combines facial landmark positioning, non-rigid registration, novel age-dependent face modelling and common distance metrics to disclose the most facial differences that vary across the time due to the subjects' age. All the experiments carried out and corresponding results presented here are based on a database comprising ordinary two-dimensional (2D) frontal face images of Down Syndrome (DS) and control sample groups. A number of craniofacial metrics have been successfully identified that highlight statistically significant and clinically relevant differences between the controls and the faces associated with DS within the age range from 1 to 18 years old, producing realistic unbiased face models with similar level of detail at all age-intervals, despite the small sample size available.

## 1 Introduction

Recently, a number of studies have been developed in order to explore associations between craniofacial differences and genetics, with notable findings in clinical face phenotype and forensic facial reconstruction [1–6]. For instance, recent works on facial metrics and imaging have improved the scientific knowledge about the genetic factors that might influence variation in facial features, providing insights into the causes of craniofacial abnormalities in genetic disorders [2–4, 7–15], as well as the feasibility of predicting human visible characteristics like facial traits from DNA [5, 6].

However, owing to the lack of age progression information, the computational analysis of such facial morphology strategies has provided a limited understanding of craniofacial development. In other words, most of these works have been based on spatial models of the face adjusted for the counter effects of age [5, 6, 15] or described as temporal exclusive population groups [2, 4, 7, 9–11, 13, 14], either consisting of only young children, adolescents, or adults' samples.

The main contribution of this work is to describe craniofacial differences based on age-related face models. More specifically, we have proposed and implemented a computational framework that combines facial landmarks positioning, non-rigid registration, novel spatio-temporal face modelling, and common distance metrics applied in clinical assessment to disclose the most significant facial differences between sample groups that vary continuously across the time due to the subjects' age. The proposed framework builds on previous multidisciplinary works applied to facial composites [16–18], medical image registration [19], brain atlas construction [20], and facial morphology [5], producing distinct face templates for distinct ages; all featured at the same spatial coordinate system and called here as face image atlases.

In order to contribute, particularly, to the growing body of recent imaging literature conveying craniofacial abnormalities in genetic disorders [11–15], we have focused our attention here on the Down Syndrome (DS) genetic disorder. DS is the most well-

known and common chromosomal disorder in humans, caused by an extra copy of chromosome 21. It is characterised by generalised growth and mental deficiency, including a distinctive and recognisable craniofacial appearance [7–10, 12, 15].

Using a database comprising ordinary two-dimensional (2D) frontal face images of DS and control sample groups from toddlers to adolescents, the computational framework proposed has been able to successfully identify a number of craniofacial metrics statistically different and clinically relevant between the controls and the faces associated with this genetic disorder.

To the best of our knowledge, our results are the first based on imaging technology that disclose continuously, at 1-year age intervals, DS morphological and developmental craniofacial changes from 1 to 18 years old, overcoming the practical limitations of small sample sizes and image acquisition artefacts when using such technology to assess the facial features in subjects with intellectual disability [11–13, 15].

The remaining sections of this paper can be summarised as follows. We provide in Section 2 a brief description of the 2D face image database used here, composed of DS and control sample groups of children aged 0–18 years. In Section 3, we explain the framework proposed to build the spatio-temporal face image atlases and extract the facial metrics used to calculate the craniofacial differences. All the experiments carried out and corresponding results are presented in Section 4 and discussed in detail in Section 5. Conclusions highlighting the main contribution of this paper and directions for further work can be found in Section 6.

## 2 Face database

Our face database contains 2D frontal images from 148 children within the age range from 0 to 18 years old. Permission for face imaging was granted by Diretoria Clinica do Hospital das Clinicas and Faculdade de Medicina da Universidade de Sao Paulo Ethics Committee (1046/09) and written parental consent was obtained

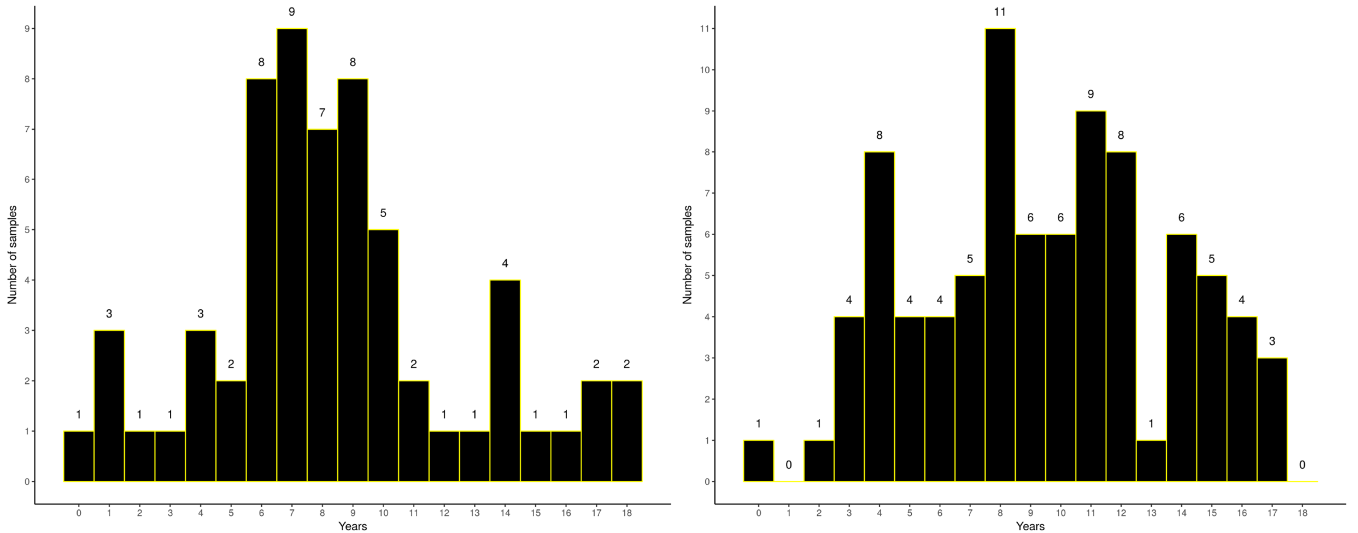


**Fig. 1** Original age (in years) histograms of the 62 DS (left) and 86 control (right) sample groups. It is important to note that the number of images are not uniformly distributed within the age range considered. For instance, at 2, 3, 12, 13, 15 and 16 years for the DS group (left histogram) and at 1, 2, 13 and 18 years for the control group (right histogram) there is either zero or only one face image originally available



**Fig. 2** Eight samples of the DS (top) and control (bottom) 2D frontal face images. To avoid the identification of the children we have masked the face images shown here with black strips

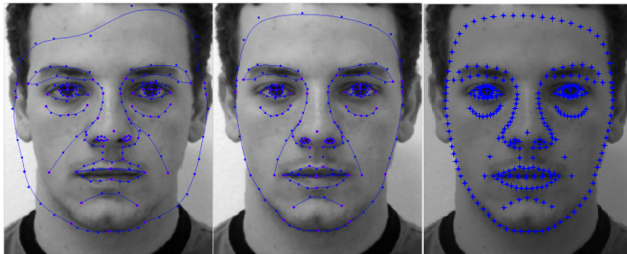


**Fig. 3** Illustration of the main steps in generating, by a friendly user interface [16], the facial landmarks on a frontal face image example [17] from the publicly available FEI Face Database [23]. For each face image, a preset total of 284 resulting landmarks are automatically obtained as shown in the right most image by sampling at equidistant positions the manually adjusted landmarks (centre image) from an initial configuration mask (left image)

prior to imaging, on a research initiative to analyse the risk of missing children [21] with disabilities in Brazil [22].

Images from two distinct and multiracial groups were analysed. The first sample group contains faces of 35 males and 27 females with DS. The second group is composed of 42 males and 44 females with no genetic disorder (controls). Fig. 1 shows the age histograms of both sample groups, where each bin represents a 1-year period of age (or, simply, age-interval).

All frontal images are greyscale, registered previously using affine transformation based on the positions of the eyes as a measure of reference, and cropped to a resolution of 280 pixels wide and 435 pixels high. Fig. 2 shows eight samples of the DS and control groups analysed in this work.

### 3 Methods

The framework proposed consists of the following four parts: facial landmarks positioning, non-rigid registration, atlas construction, and craniofacial metrics location. It extends and generalises our previous and preliminary works [17, 18] of generating photo-realistic facial changes and age-dependent face atlas. All these parts are described in detail in the following sub-sections.

#### 3.1 Facial landmarks positioning

The shape of each face needs first to be characterised by a set of landmarks (or fiducial points) placed on the 2D frontal face images. These determine a feature correspondence that enables the subsequent non-rigid alignment of all face images.

The landmark placement of each face image has been achieved by using the following friendly user interface [16]. Initially, a face is localised within an image by placing manually a point at the centre of the left eye, centre of the right eye, and the lowest point on the chin. A geometric transformation, based on the positions of these three anatomical points, is then applied to a standard point model [16]. The transformed model is placed automatically on the image as an initial configuration mask, thereby approximately delineating the salient internal features and the perimeter of the face (Fig. 3, left image). Polynomial curves are placed on the corresponding feature boundaries by manually adjusting up to 61 points of this mask as required (Fig. 3, centre image). Joins between polynomial curve segments are identified by points with magenta borders. To increase smoothness, additional fiducial points are automatically generated by sampling at equidistant positions along the polynomial curves that interpolate the landmarks. For each face image, a preset total of 284 resulting landmarks are obtained as illustrated in the right most image of Fig. 3.

In this work, however, the 24 points associated with the hairline were not used, because they are not related to the craniofacial metrics applied here. Therefore, the shape of each face has been represented by the total number of 260 landmarks.

#### 3.2 Non-rigid registration

We have adapted the free-form deformation (FFD) [24, 25] algorithm proposed by Rueckert *et al.* [19] successfully in the context of 3D medical images [26] to non-rigidly register all the face images [17, 27, 28].

In this 2D version of the non-rigid registration algorithm, the input (or source) image is represented through a set of points, as follows:

$$\Omega_{\text{source}} = \{(x, y) | 0 \leq x < h_x, 0 \leq y < h_y\}, \quad (1)$$

---

```

Define  $k$ , tolerance value
Define  $\Delta\sigma$ , kernel width change
Set  $\bar{N}$  to the median of all  $N_t$  age-intervals
foreach age-interval  $t$  do
  Set  $N_t^*$  to the original number of images at  $t$ 
  Set  $\varphi_t$  as the set of original images at  $t$ 
  Set  $\varphi_{t-1}$  as the set of original images at  $t-1$ 
  Set  $\varphi_{t+1}$  as the set of original images at  $t+1$ 
  Set  $\sigma_t = 1$ 
  while ( $N_t^* \leq \bar{N} + k$ ) and ( $\varphi_{t-1}$  or  $\varphi_{t+1} \neq \{\}$ ) do
     $flag = 0$ 
    if  $\varphi_{t-1} \neq \{\}$  then
      Add to  $\varphi_t$  a neighbor image from  $\varphi_{t-1}$ 
      Remove from  $\varphi_{t-1}$  the image added
       $N_t^* = N_t^* + 1$ 
       $flag = 1$ 
    if  $\varphi_{t+1} \neq \{\}$  then
      Add to  $\varphi_t$  a neighbor image from  $\varphi_{t+1}$ 
      Remove from  $\varphi_{t+1}$  the image added
       $N_t^* = N_t^* + 1$ 
       $flag = 1$ 
    if  $flag \neq 0$  then
       $\sigma_t = \sigma_t \times (1 + \Delta\sigma)$ 

```

---

**Fig. 4** Illustration of the pairwise non-rigid registration process for construction of the spatio-temporal face image atlas at age-interval  $t$ . Analogously to Fig. 2, in order to avoid the identification of the subjects we have masked with black strips all the original images shown here

where  $h_x$  and  $h_y$  denote the width and height in pixels of the image, respectively. It also requires a mesh  $\Phi_{\text{source}}$  of  $n_x \times n_y$  control points (or resolution), where  $1 \leq n_x \leq h_x$  and  $1 \leq n_y \leq h_y$ , with the control points  $\phi_{xy}$  belonging to the domain  $\Omega_{\text{source}}$ .

The goal is to register a source image with a target one by minimising the misalignment of the landmarks from the former to the landmarks of the latter. At the beginning, the algorithm performs a global alignment between the landmarks of the source image and the corresponding ones of the target image, using affine transformation [19, 29]. Next, an iterative coarse-to-fine processing is applied, where the initial control point mesh  $\Phi_{\text{source}}$  is subsequently refined with increasing resolution until its control points achieve the spatial positions that satisfy the alignment criterion. The computational complexity of this registration method is linearly related to the resolution of the control point mesh used.

The alignment criterion adopted here is the squared distance between the two sets of landmarks. More specifically, the new position of a point at the location  $(x, y)$  can be calculated by the function  $f(x, y)$  below using  $4 \times 4$  neighbouring control points [30] and tensor product of B-splines [25], as follows:

$$f(x, y) = \sum_{k=0}^3 \sum_{l=0}^3 B_k(s_x) B_l(s_y) \phi_{(i+k)(j+l)}, \quad (2)$$

where  $i = \lfloor x/n_x \rfloor - 1$ ,  $j = \lfloor y/n_y \rfloor - 1$ ,  $s_x = x - \lfloor x/n_x \rfloor$ , and  $s_y = y - \lfloor y/n_y \rfloor$ .  $B_k(s_x)$  and  $B_l(s_y)$  correspond to cubic B-spline functions evaluated, respectively, at  $s_x$  and  $s_y$  and defined as [25]:

$$B_0(u) = (-u^3 + 3u^2 - 3u + 1)/6,$$

$$B_1(u) = (3u^3 - 6u^2 + 4)/6,$$

$$B_2(u) = (-u^3 + 3u^2 + 3u + 1)/6,$$

$$B_3(u) = u^3/6,$$

where  $0 \leq u < 1$  [25]. This allows more flexible non-uniform control point spacing and smoother deformations.

The multi-resolution computational strategy has been applied because a range of facial deformations might be necessary, varying

from holistic ones, which are large, more global, and consequently can only be achieved by using coarse control point spacing (or low mesh resolution), to featural ones, which are more detailed, localised, requiring then finer spacing (or high mesh resolution). The final deformation fields of each source image are generated when achieving the finest level of the FFD resolution.

### 3.3 Atlas construction

The novel spatio-temporal face models have been built using a pairwise normalisation process proposed in [20] for human brain neuroimage analysis. Fig. 4 illustrates schematically the main idea of this process, extended and generalised here for face image analysis.

For each age-interval  $t$  with  $N_t$  total number of images, we select one image  $i$  as source and the remaining images as targets, running a number of  $N_t \times (N_t - 1)$  pairwise registrations. The  $(N_t - 1)$  transformations of all  $N_t$  source images are averaged out

$$\bar{T}_i = \frac{1}{(N_t - 1)} \sum_{\substack{j=1 \\ j \neq i}}^{N_t} T_{i,j} \quad (3)$$

and applied to the corresponding source images

$$\bar{I}_i = I_i \circ \bar{T}_i^{-1} \quad (4)$$

to generate their non-rigidly registered mean images, as shown in Fig. 4, for  $i = 1, \dots, N_t$ . The standard spatio-temporal face image atlas at age-interval  $t$ ,  $\mathcal{A}(t)$ , is calculated by averaging all the  $N_t$  mean images

$$\mathcal{A}(t) = \frac{1}{N_t} \sum_{i=1}^{N_t} \bar{I}_i. \quad (5)$$

It is clear from (5) that each mean image  $\bar{I}_i$  has the same importance in the composition of the spatio-temporal face image atlas. In other words, the  $N_t$  mean images are equally weighted, because all of them belong to the same age-interval  $t$ . However, as illustrated in the previous Fig. 1 of the original age histograms, the number of images are not uniformly distributed over the age-interval range considered and, in fact, there are some age-intervals with zero or only one sample available.

Hence, it would be valid to attempt to equalise the total number of images among all age-intervals, using some weighted support from temporal neighbours [20] to allow the calculation of spatio-temporal face image atlases properly at any age-interval  $t$ .

Let  $w(t_i, t)$  be the weight assigned to the image  $i$  at the age-interval  $t$  given by a Gaussian kernel [20]:

$$w(t_i, t) = \frac{1}{\sigma_t \sqrt{2\pi}} \exp \frac{-(t_i - t)^2}{2\sigma_t^2}, \quad (6)$$

where  $t_i$  denotes the age in years of the subject at image  $i$ ,  $t$  is the age-interval in years within the range considered, and  $\sigma_t$  corresponds to the kernel width at  $t$ . The parameter  $\sigma_t$  would allow neighbouring images to contribute with different weights at different age-intervals.

Algorithm 1 (Fig. 5) has been proposed and implemented to increase, using the nearest  $t \pm 1$  neighbours, whenever necessary and possible, the number of original images  $N_t$  to  $N_t^*$ , where  $N_t^* \geq N_t$ , and estimate the kernel width parameter, where  $\sigma_t \geq 1$ . It is analogous to the algorithm proposed in [20] with the rationale here that at age-intervals with relatively fewer number of images, relatively larger kernel width might be chosen [20]. The tolerance value  $k$  and kernel width change  $\Delta\sigma$  might be chosen experimentally.

Thus, the weighted version of the spatio-temporal face image atlas at age-interval  $t$ ,  $\mathcal{A}^*(t)$ , can then be calculated as

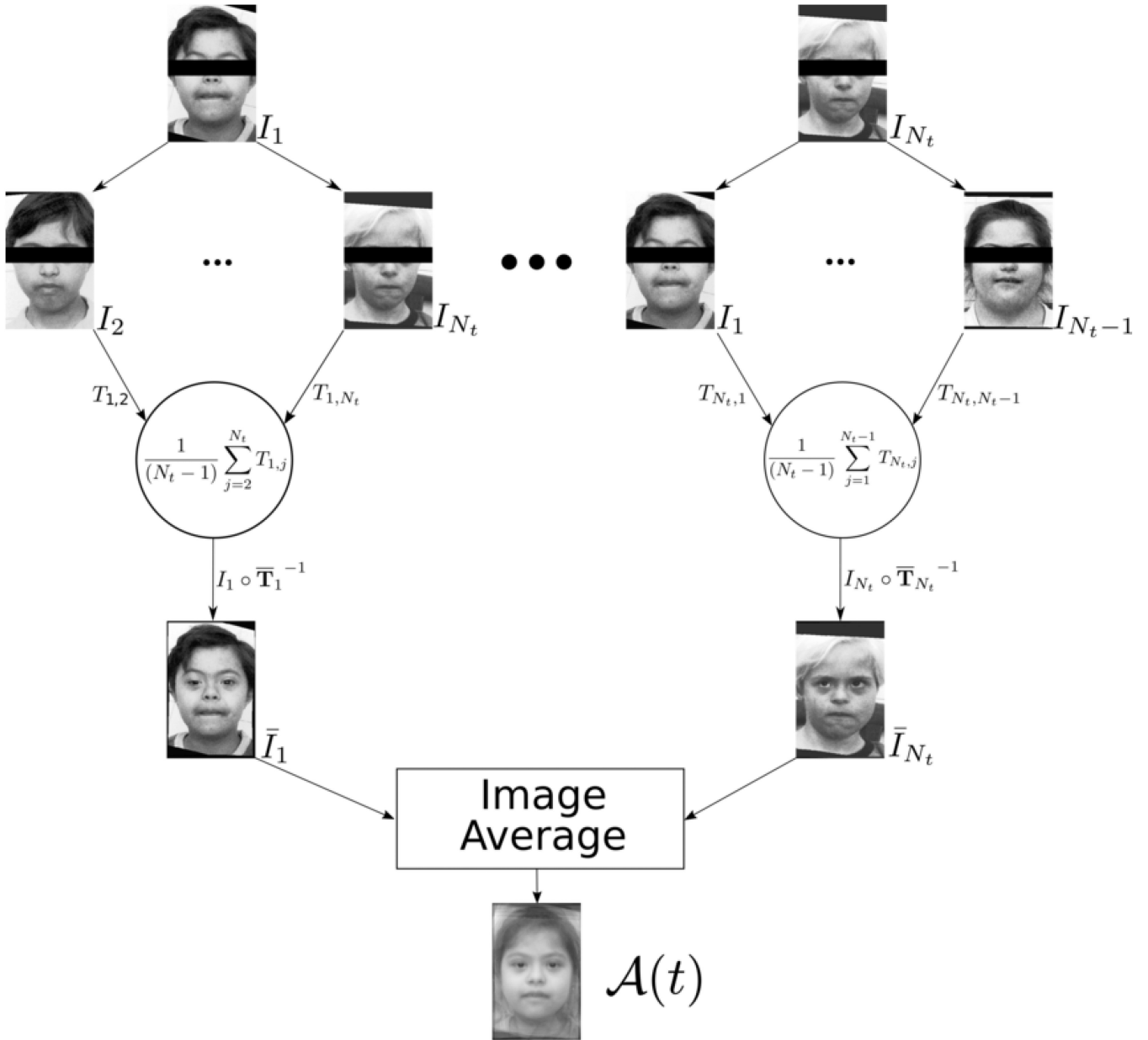


Fig. 5 Algorithm 1: Estimation of  $N_t^*$  and  $\sigma_t$

$$\mathcal{S}^*(t) = \frac{1}{\sum_{i=1}^{N_t^*} w(t_i, t)} \sum_{i=1}^{N_t^*} w(t_i, t) \bar{I}_i, \quad (7)$$

where  $w(t_i, t)$  is given by (6).

### 3.4 Craniofacial metrics

We have used a set of craniofacial metrics commonly applied in clinical assessment to describe the most significant spatio-temporal changes of the non-rigidly registered 2D face images [4–6, 31, 32].

Fig. 6 illustrates the 12 craniofacial measurements used in this work, grouped together to describe the following anthropometric regions particularly concerned with DS [15]: **face** (top row: A, B, C, D); **nose** (middle row: E, F, G, H); **mouth and lips** (bottom row: I, J, K, L).

All these metrics have been calculated using the 2D locations of the corresponding landmarks saved after the pairwise non-rigid registration of each face image.

## 4 Experimental results

We have applied the algorithm previously described in Section 3.3 to increase the total number of face images for both DS and control

sample groups within each age-interval and generate the weighted version of the spatio-temporal face image atlases. The median  $\bar{N}$  of the original number of images at each age-interval of the DS and control samples are, respectively, 2 and 4. We have set here  $k = 4$  for the DS sample group and  $k = 3$  for the control one to have a feasible number of face images for every age-interval, and determined the kernel width change experimentally, equals to  $\Delta_\sigma = 0.3$  for both sample groups.

Fig. 7 shows the equalised age histograms of the DS (left) and control (right) augmented sample groups. All the age-varying Gaussian kernels are also illustrated, shown centralised on the corresponding 1-year spans. We can see that, unlike the original age histograms previously described in Fig. 1, the number of samples per age-interval is now more uniformly distributed over the age range in both sample groups. For example, at age-interval  $t = 5$ , there were originally (left histogram of Fig. 1) only two face images available for the DS sample group. After the equalisation algorithm, it is now possible to consider at  $t = 5$  a set of eight face images in total (left histogram of Fig. 7), composed of the two originals with maximum weight ( $w = 1$ ) and the other six using the nearest  $t = 4$  and  $t = 6$  neighbours, but with non-maximum weights ( $w < 1$ ). Analogously, at age-interval  $t = 13$ , there was originally only one face image available for the control sample

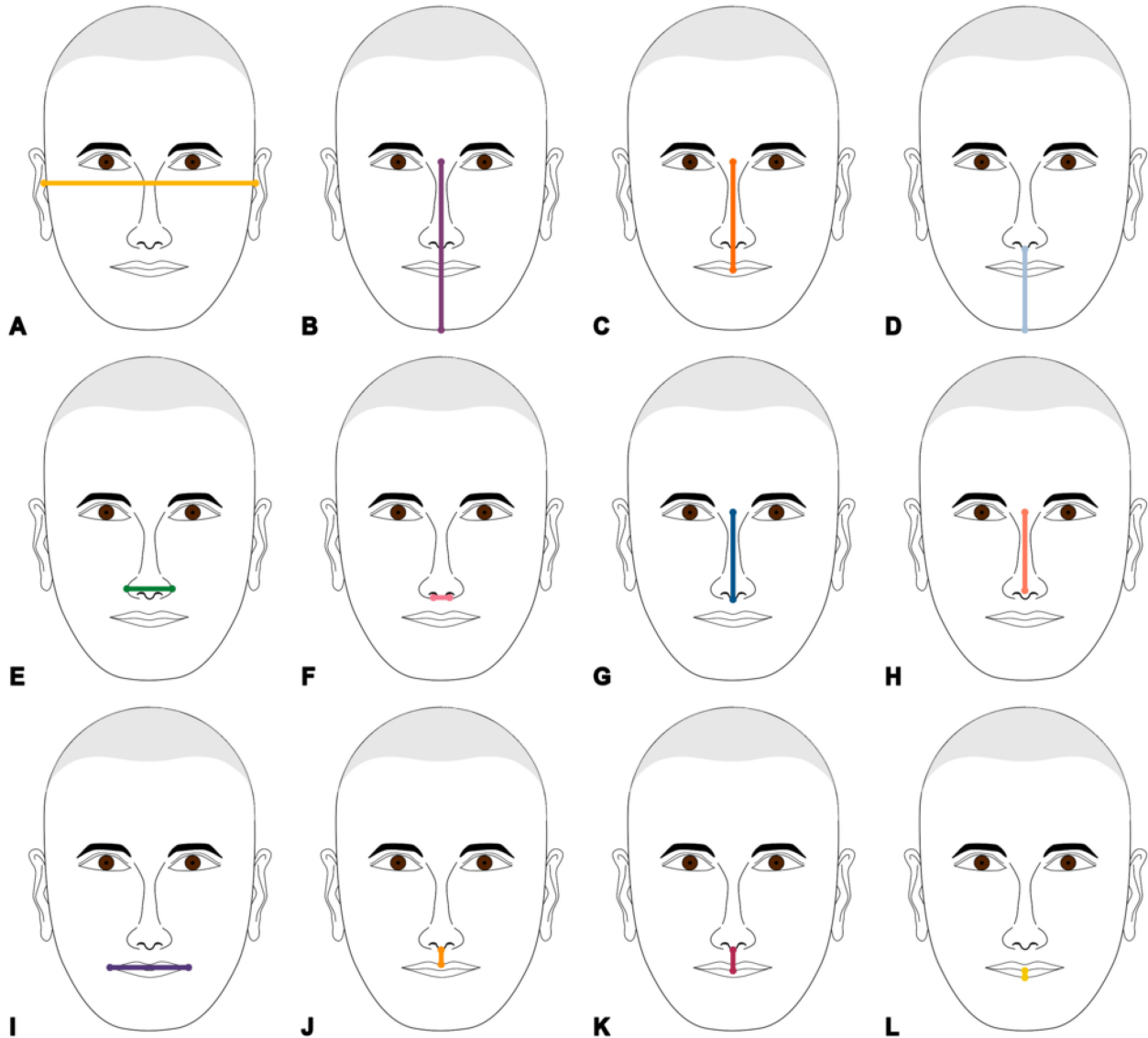


**Fig. 6** Set of 12 frontal craniofacial metrics used in this work and grouped together according to their corresponding regions: **face** (top row) (A) Cranial base width, (B) Morphological facial height, (C) Upper facial height, (D) Lower facial height; **nose** (middle row), (E) Nasal width, (F) Subnasal width, (G) Nasal height, (H) Nasal bridge length; **mouth and lips** (bottom row), (I) Labial fissure length, (J) Philtrum length, (K) Upper lip height; and (L) Lower lip height. All these 12 metrics are facial anthropometric measurements concerned with DS

group (right histogram of Fig. 1). After the equalisation algorithm, it is now possible to consider nine face images in total at this age-interval (right histogram of Fig. 7), taking into account distinct weights given by the corresponding age-varying Gaussian kernel. These comparable numbers of face images for each age-interval provide atlases of both sample groups with similar level of detail at all age-intervals.

Fig. 8 shows the resulting spatio-temporal face image atlases from  $t = 1$  (left) to  $t = 18$  (right) years. The first two rows, from top to bottom, illustrate the standard  $\mathcal{A}(t)$  and weighted  $\mathcal{A}^*(t)$  atlases of the DS subjects using, respectively, the original and augmented samples. Likewise, in the last two rows, from top to bottom, the  $\mathcal{A}(t)$  spatio-temporal face image atlases of the control subjects using the original samples are visually compared with the  $\mathcal{A}^*(t)$  ones composed of augmented samples with age-varying weights. Since at 2, 3, 12, 13, 15, and 16 years for the DS group (first row) and at 1, 2, 13, and 18 years for the control group (third row) there is either zero or only one face image originally available, the corresponding  $\mathcal{A}(t)$  cannot be calculated, leaving the standard atlas construction with inconsistencies across time and more sensitive to the choice of face images at age-intervals with small sample sizes. In contrast, the weighted version of the spatio-temporal atlases  $\mathcal{A}^*(t)$  based on the augmented sample groups allow the construction of atlases of both sample groups (second

and forth rows) at all age-intervals continuously, with consistent level of detail at every 1-year period of age.

We have performed unpaired two-sample t-tests with pooled variance estimate to compare statistically the facial metrics between the sample groups for each age-interval. Fig. 9 highlights, from top to bottom and left to right, the statistically different ( $p < 0.05$ ) facial metrics across time between the DS and control corresponding augmented sample groups. Based on such statistical analysis, the most discriminant facial metrics are: nasal height (G: 14 occurrences out of 18), nasal bridge length (H: 11/18), upper facial height (C: 10/18), lower facial height (D: 10/18), and cranial base width (A: 10/18). The least discriminant ones are: morphological facial height (B: 4/18), subnasal width (F: 5/18), labial fissure length (I: 5/18), philtrum length (J: 5/18), upper lip height (K: 5/18), and lower lip height (L: 5/18).

## 5 Discussion

Our 2D imaging results are related with the DS craniofacial differences in the following frontal anthropometric regions: face, nose, and mouth and lips. A number of recent studies [10, 11, 13–15] have addressed DS morphological craniofacial changes in such regions using digital imaging technology as well. However, our work is the first to propose and implement a computational framework that discloses the developmental changes of these

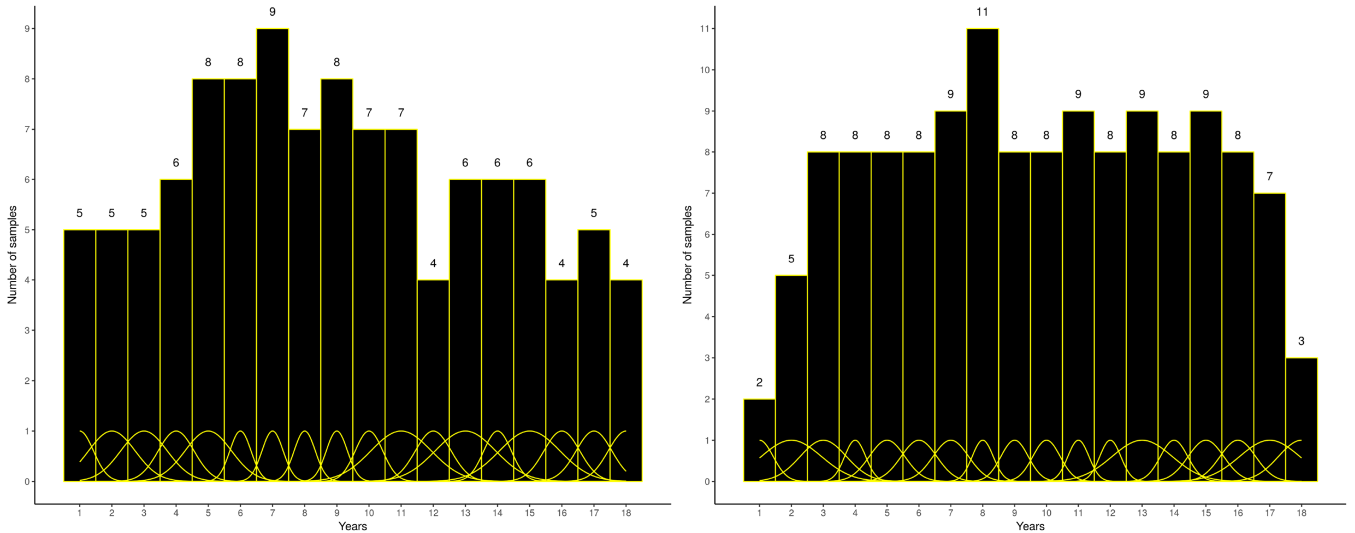


**Fig. 7** Equalised age (in years) histograms of the augmented DS (left) and control (right) sample groups. All age-varying Gaussian kernels are also shown on the corresponding 1-year period spans. Compared to the previous Fig. 1, it is possible to see that the number of samples per age-interval is now more uniformly distributed within the age range considered in both sample groups

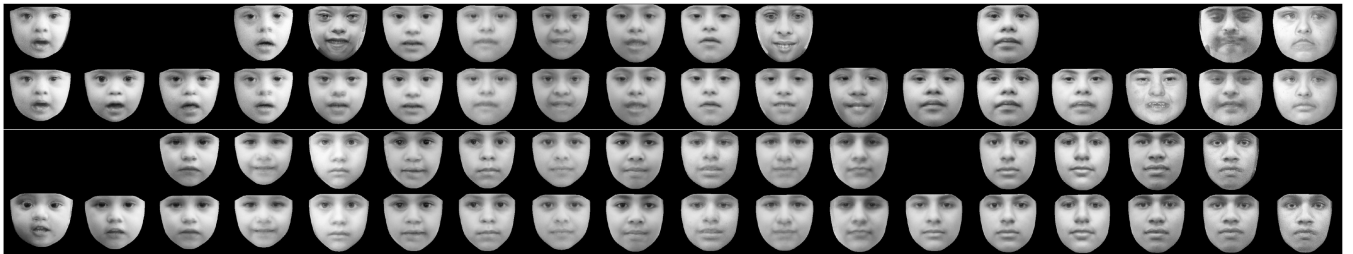


**Fig. 8** Resulting standard  $\mathcal{A}(t)$  and weighted  $\mathcal{A}^*(t)$  spatio-temporal atlases from  $t = 1$  (left) to  $t = 18$  (right) years. From top to bottom:  $\mathcal{A}(t)$  atlases of DS subjects using the original samples;  $\mathcal{A}^*(t)$  atlases of DS subjects using the augmented samples;  $\mathcal{A}(t)$  atlases of control subjects using the original samples; and  $\mathcal{A}^*(t)$  atlases of control subjects using the augmented samples

differences, at 1-year age intervals, continuously across the age range from 1 to 18 years old, providing insights about these underlying craniofacial features in DS owing to age progression.

Overall, our experimental results have indicated that the most discriminant region within the entire age range considered is the face region. This region captures essentially the global shape of the faces, showing distinctive facial length ( $C$ : upper facial height;  $D$ : lower facial height) and width ( $A$ : cranial base width) between the DS and control sample groups analysed. These are actually common craniofacial aspects found in the clinically related literature [9, 10, 12, 15, 33], because faces of subjects with DS are expected to be narrower and shorter than the faces of control subjects.

Hence, not surprisingly, our findings have also showed that the second most discriminant region is the nose region, with particular highlight to the nasal length ( $G$ : nasal height;  $H$ : nasal bridge length), but not its width ( $E$ : nasal width;  $F$ : subnasal width), indicating that a shorter face implies here shorter facial as well as nasal heights in subjects with DS.

Additionally, our experimental results have showed that the mouth and lips is the least statistically different region considered here, because each one of its four metrics has been discriminant only in 5 out of 18 occurrences possible given the 1-year period of interval. According to the related literature [10, 12, 15, 33], DS faces might exhibit some degree of dysmorphology in this region, essentially a general decreased mouth width with prominent lips [12]. We have found statistical differences on the labial fissure length ( $I$ ), which is an equivalent metric to mouth width, at  $t(I) = \{1, 9, 10, 13, 15\}$ , and differences on the philtrum length ( $J$ ), upper lip height ( $K$ ) and lower lip height ( $L$ ) at, respectively,  $t(J) = \{5, 6, 7, 8, 11\}$ ,  $t(K) = \{2, 3, 4, 7, 12\}$ , and  $t(L) = \{2, 3, 4, 5, 12\}$ . However, these changes have not been consistently present all over the age range considered, suggesting an age-specific behaviour. Interestingly, though, such few

craniofacial differences are predominantly present at the youngest ages (from 1 to 4 years), become irregular with increasing age (from 5 to 15 years), and disappear at the oldest ages considered (from 16 to 18 years), indicating that these features might grow in the same proportion in both DS and controls during the final period of adolescence.

Although our findings have described differences at all age-intervals, the maximum number of craniofacial changes happened at  $t = 5$  and  $t = 13$ , with eight statistical differences present out of 12 metrics considered. These age-intervals, especially around 3–5 years and 13–15 years, are peculiar to the well-known observed acceleration periods of facial development [31, 34], configuring the transition periods from toddlers to children and from children to adolescents.

Our study addresses two practical limitations in the current imaging-related literature to studying craniofacial changes across a wide range of ages [11–13, 15]. Despite the fact that our experimental results encompass a relatively large total number of images, equals to 148 samples (62 DS and 86 controls), these images have not been uniformly distributed over the age range considered (from 1 to 18 years old). In fact, we have shown that there were some age-intervals originally with zero or only one sample available. Our imaging framework has overcome this limitation, addressing the small sample size issue with the novel atlas construction method described, which allows the calculation of spatio-temporal face image atlases properly at all age-intervals using weighting information from temporal neighbours. Moreover, since the atlas construction has been based on a pairwise non-rigid normalisation process, it also minimises typical acquisition and motion image artefacts. These artefacts are quite common limitations to applying imaging technology, because it would rely on the subjects to staying still and maintaining a neutral facial expression while being photographed. In situations that involve subjects with intellectual disability, such motionless and

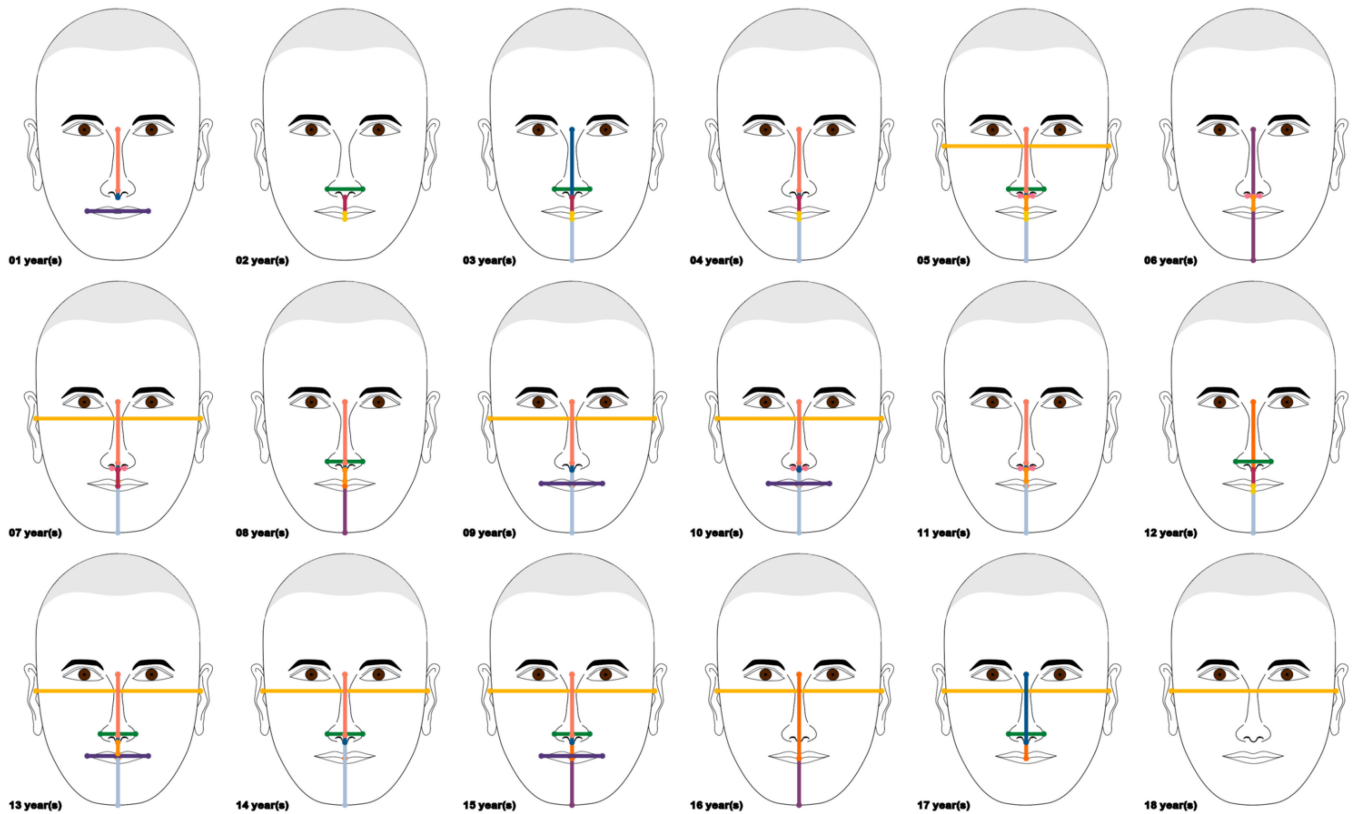


**Fig. 9** Statistically different facial metrics between the DS and control corresponding augmented sample groups. From top to bottom and left to right, the significant changes ( $p < 0.05$ ) for each age-interval are: GHI (1 yr); EKL (2 yrs); DEGKL (3 yrs); DGHKL (4 yrs); ADEFGHJL (5 yrs); BFJ (6 yrs); ADFGHJK (7 yrs); BCEGHJ (8 yrs); ACDGHI (9 yrs); ACDFGHI (10 yrs); CDFGHJ (11 yrs); CDEKL (12 yrs); ACDEGHJI (13 yrs); ACDEGH (14 yrs); ABCEGHI (15 yrs); ABC (16 yrs); ACEG (17 yrs); and A (18 yrs)

expressionless behaviour might be very difficult to achieve in practice.

## 6 Conclusion

This work proposes and implements a computational framework to describe craniofacial differences based on spatio-temporal face image atlases. The framework produces realistic unbiased face models with similar level of detail at all age-intervals, despite the small sample size available for each age-interval considered. All the experiments have been based on ordinary 2D frontal face images, irrespective of the subject's gender or ethnicity. Using a face database composed of DS and control sample groups within the age range from toddlers to adolescents, a number of craniofacial differences clinically relevant have been statistically highlighted across the time due to such genetic disorder.

Further work on larger data sets would definitely increase the statistical power of the inferring spatio-temporal face image atlases, allowing the integration of the craniofacial metrics with genetic data for possible use in clinical settings and genome-wide association studies. Given the most significant facial metrics extracted spatially and across the age, future work might also investigate how specific genetic variants relate to the phenotypic behaviour of these traits in DS facial ageing. Nevertheless, the applicability of the framework proposed is generic, not restricted to DS, and might be helpful to broaden the understanding of dysmorphic craniofacial development of other genetic disorders, like Apert, Progeria, and Williams-Beuren syndromes.

## 7 Acknowledgment

The authors would like to thank the financial support provided by CAPES (PROSUC, code 001), FAPESP (2012/22377-6) and CNPq (309532/2014-0). This work is part of the Newton Advanced Fellowship (NA140147) appointed by the Royal Society to Carlos E. Thomaz.

## 8 References

- [1] Kayser, M., Schneider, P.M.: 'DNA-based prediction of human externally visible characteristics in forensics: motivations, scientific challenges, and ethical considerations', *Forensic Sci. Int. Genetics*, 2009, **3**, pp. 154–161
- [2] Peng, S., Tan, J., Hu, S., *et al.*: 'Detecting genetic association of common human facial morphological variation using high density 3D image registration', *PLoS Comput. Biol.*, 2013, **9**, pp. 1–11
- [3] Ferry, Q., Steinberg, J., Webber, C., *et al.*: 'Diagnostically relevant facial gestalt information from ordinary photos', *Elife*, 2014, **3**, pp. 1–22
- [4] Adhikari, K., Fuentes-Guajardo, M., Quinto-Sanchez, M., *et al.*: 'A genome-wide association scan implicates DCHS2, RUNX2, GLI3, PAX1 and EDAR in human facial variation', *Nat. Commun.*, 2016, **7**, pp. 1–11
- [5] Shaffer, J.R., Orlova, E., Lee, M.K., *et al.*: 'Genome-wide association study reveals multiple loci influencing normal human facial morphology', *PLoS Genet.*, 2016, **12**, pp. 1–21
- [6] Lee, M.K., Shaffer, J.R., Leslie, E.J., *et al.*: 'Genome-wide association study of facial morphology reveals novel associations with FREM1 and PARK2', *PLOS One*, 2017, **12**, pp. 1–13
- [7] Quintanilla, J.S., Biedma, B.M., Rodriguez, M.Q., *et al.*: 'Cephalometrics in children with down's syndrome', *Pediatr. Radiol.*, 2002, **32**, pp. 635–643
- [8] Ferrario, V.F., Dellavia, C., Zanotti, G., *et al.*: 'Soft tissue facial anthropometry in down syndrome subjects', *J. Craniofacial Surg.*, 2004, **15**, pp. 528–532
- [9] Suri, S., Tompson, B.D., Cornfoot, L.: 'Cranial base, maxillary and mandibular morphology in down syndrome', *Angle Orthod.*, 2010, **80**, pp. 861–869
- [10] Starbuck, J., Reeves, R.H., Richtsmeier, J.: 'Morphological integration of soft-tissue facial morphology in down syndrome and siblings', *Am. J. Phys. Anthropol.*, 2011, **146**, pp. 560–568
- [11] Zhao, Q., Okada, K., Rosenbaum, K., *et al.*: 'Digital facial dysmorphology for genetic screening: Hierarchical constrained local model using ICA', *Med. Image Anal.*, 2014, **18**, pp. 699–710
- [12] Sforza, C., Dolci, C., Dellavia, C., *et al.*: 'Abnormal variations in the facial soft tissues of individuals with down syndrome: Sudan versus Italy', *Cleft Palate Craniofac. J.*, 2015, **52**, pp. 588–596
- [13] Kruszka, P., Porras, A.R., Sobering, A.K., *et al.*: 'Down syndrome in diverse populations', *Am. J. Med. Genetics A*, 2016, **173**, pp. 42–53
- [14] Cerrolaza, J.J., Porras, A.R., Mansoor, A., *et al.*: 'Identification of dysmorphic syndromes using landmark-specific local texture descriptors'. 2016 IEEE 13th Int. Symp. on Biomedical Imaging (ISBI), Prague, Czech Republic, 2016, pp. 1080–1083
- [15] Jayaratne, Y.S.N., Elsharkawi, I., Macklin, E.A., *et al.*: 'The facial morphology in down syndrome: A 3D comparison of patients with and without obstructive sleep apnea', *Am. J. Med. Genetics A*, 2017, **173**, pp. 3013–3021

- [16] Gibson, S.J.: 'EigenFIT: A Statistical Learning Approach to Facial Composites'. PhD thesis, University of Kent, 2006
- [17] Xavier, I., Pereira, M., Giraldi, G., *et al.*: 'A photo-realistic generator of most expressive and discriminant changes in 2D face images'. 2015 Sixth Int. Conf. on Emerging Security Technologies (EST), Braunschweig, Germany, 2015, pp. 80–85
- [18] Xavier, I., Giraldi, G., Gibson, S., *et al.*: 'Construction of a spatio-temporal face atlas: experiments using down syndrome samples'. Conf. on Graphics, Patterns and Images (SIBGRAPI):Workshop on Face Processing Applications, Sao Paolo, Brazil, 2016, pp. 1–4
- [19] Rueckert, D., Sonoda, L.I., Hayes, C., *et al.*: 'Nonrigid registration using free-form deformations: application to breast MR images', *IEEE Trans. Med. Imaging*, 1999, **18**, (8), pp. 712–721
- [20] Serag, A., Aljabar, P., Ball, G., *et al.*: 'Construction of a consistent highdefinition spatio-temporal atlas of the developing brain using adaptive kernel regression', *NeuroImage*, 2012, **59**, pp. 2255–2265
- [21] Morewitz, S.J., Colls, C.S.: '*Handbook of missing persons*' (Springer, Cham, Switzerland, 2016)
- [22] Gattas, G.J.F., Figaro-Garcia, C., Thomaz, C.E., *et al.*: 'The risk of missing children and adolescents with disabilities: a Brazilian experience'. Int. Conf. on Forensic Research & Technology, Chicago, 2012, Vol. 3, pp. 71–71
- [23] Thomaz, C.E., Giraldi, G.A.: 'A new ranking method for principal components analysis and its application to face image analysis', *Image Vis. Comput.*, 2010, **28**, pp. 902–913
- [24] Sederberg, T.W., Parry, S.R.: 'Free-form deformation of solid geometric models'. Proc. of SIGGRAPH'86, Computer Graphics, Dallas, TX, USA, 1986, pp. 151–160
- [25] Lee, S., Wolberg, G., Chwa, K., *et al.*: 'Image metamorphosis with scattered feature constraints', *IEEE Trans. Vis. Comput. Graphics*, 1996, **2**, (4), pp. 337–354
- [26] Klein, A., Andersson, J., Ardekani, B.A., *et al.*: 'Evaluation of 14 nonlinear deformation algorithms applied to human brain mri registration', *NeuroImage*, 2009, **46**, pp. 786–802
- [27] Koelstra, S., Pantic, M.: 'Non-rigid registration using free-form deformations for recognition of facial actions and their temporal dynamics'. 8th IEEE Int. Conf. on Automatic Face & Gesture Recognition, 2008. FG'08, Amsterdam, The Netherlands, 2008, pp. 1–8
- [28] Koelstra, S., Pantic, M., Patras, I.: 'A dynamic texture-based approach to recognition of facial actions and their temporal models', *IEEE Trans. Pattern Anal. Mach. Intell.*, 2010, **32**, pp. 1940–1954
- [29] Schnabel, J.A., Rueckert, D.: 'A generic framework for non-rigid registration based on non-uniform multi-level free-form deformations'. Proc. of Medical Image Computing and Computer-Assisted Intervention (MICCAI), Utrecht, The Netherlands, 2001, pp. 573–581
- [30] Lee, S., Wolberg, G., Shin, S.Y.: 'Scattered data interpolation with multilevel bsplines', *IEEE Trans. Vis. Comput. Graphics*, 1997, **3**, pp. 228–244
- [31] Farkas, L.G., Munro, I.R.: '*Anthropometric facial proportions in medicine*' (Charles C Thomas, Springfield, IL, USA, 1987)
- [32] George, R.M.: '*Facial geometry: graphic analysis for forensic artists*' (Charles C Thomas, Springfield, IL, USA, 2007)
- [33] Ferrario, V.F., Dellavia, C., Colombo, A., *et al.*: 'Three-dimensional assessment of nose and lip morphology in subjects with down syndrome', *Ann. Plast. Surg.*, 2004, **53**, pp. 577–583
- [34] Fu, Y., Guo, G., Huang, T.S.: 'Age synthesis and estimation via faces: A survey', *IEEE Trans. Pattern Anal. Mach. Intell.*, 2010, **32**, pp. 1955–1976